Power matrix assessment and extreme loads estimation on a flap type wave energy converter in front of a dike

Virginie Baudry, Salvatore Marrone, Aurélien Babarit, David Le Touzé, Alain H. Clément

Power matrix assessment and extreme loads estimation on a flap type wave energy converter in front of a dike

Virginie Baudry[#1], Salvatore Marrone[*2], Aurélien Babarit[#3], David Le Touzé[#4], Alain H. Clément[#5]

[#] *Ecole Centrale de Nantes – LHEEA, UMR CNRS 6598 - 1 rue de la Noé, BP 92101, 44321 Nantes Cédex 3, France*

[1]virginie.baudry@ec-nantes.fr , [3]aurelien.babarit@ec-nantes.fr, [4]david.letouze@ec-nantes.fr, [5]alain.clement@ec-nantes.fr

[*] *CNR INSEAN – Via di Vallerano 139, 00128 Roma, Italy*

[2]salvatore.marrone@cnr.it

***Abstract*— The EMACOP (Marine Energies in coastal regions and harbours) project aims at studying the feasibility and relevance of combining wave energy converters (WEC) with coastal structures such as dikes. In the framework of this project, we present in this paper a complementary use of a potential code and a SPH code for the study of a bottom-mounted pitching flap. The developed tools are applied to Bayonne and Saint Jean de Luz site in order to evaluate mean annual power production and estimate maximum loads experienced by the flap under extreme wave conditions. Regarding the power matrix assessment, the specificity of the study is in the use of symmetry considerations to model the behaviour of the flap in front of the dike. The advantage of coupling with the dike compared with an isolated configuration on WEC performances is analysed and main uncertainties are mentioned. In parallel to the WEC performance assessment, SPH computations have been performed to estimate extreme loads experienced by the flap. The influence of wave breaking inception and tide level on impact loads is addressed, and 3D effects are highlighted.**

***Keywords*— Wave energy converter, Boundary Element Method, power matrix, SPH, wave impact**

I. INTRODUCTION

The EMACOP (Marine Energies in coastal regions and harbours) project aims at studying the feasibility and relevance of combining wave energy converters (WEC) with coastal structures such as dikes.

As part of the project, tools aiming at estimating the energy yields of four different generic WECs with various working principles including overtopping devices, pitching flaps, heaving buoys and oscillating water columns coupled with a breakwater are currently being developed. The survivability of those wave energy converters combined to coastal structures is another important issue of the EMACOP project to assess the feasibility of such projects in coastal regions.

In this paper, we present a complementary use of a potential code and a SPH code for the study of a bottom-mounted pitching device consisting of a partly submerged flap placed in front of a breakwater. Several numerical researches and studies on bottom mounted pitching flap behaviour have recently been reported. For example, Babarit et al [1] have been assessing numerically the power matrix of a bottom-mounted pitching flap. Sarkar and al. have been studying the wave power absorption of a flap –type WEC near a straight coast, using an analytical model [2].

The specificity of the numerical 3D potential method developed to assess the power matrix of the WEC lies in the use of symmetry considerations to model the flap in front of a dike. Then, the numerical tool is applied to Saint Jean de Luz and Bayonne sites (South west Atlantic coast, France) in order to evaluate the mean annual power production, and the benefit from dike reflections on power absorption is analysed. In parallel to the study of the performances of the device in terms of power production, SPH computations have been performed to estimate maximum loads experienced by the flap under extreme wave conditions in front of Tarnos dike, in Bayonne site. Effects of parameters such as wave breaking inception, and tide level on impact loads have been studied within the 2D SPH simulations. 3D effects and associated repercussion on critical loads are highlighted for the most relevant impact case, when the impact occurs at the breaking inception.

The present paper is divided into 3 sections: section **II** is dedicated to the description of the configuration and characteristics of the flap, section **III** presents the power matrix assessment of the flap placed in front of a vertical dike, section IV presents the estimation of the extreme loads on the flap using SPH method, and section V is the conclusion.

II. CONFIGURATION AND MAIN CHARACTERISTICS OF THE FLAP TYPE PITCHING WECS

The device is a simple pitching flap oscillating about a fixed axis close to the sea bottom. The working principle of the studied flap type pitching WEC is directly inspired from that of the Oyster device which geometry has been adapted to Bayonne and Saint Jean de Luz site bathymetry.

A. Pitching WEC characteristics and configurations

The main dimensions and characteristics of the flap type pitching WEC are given in table I for Bayonne and Saint Jean de Luz configuration. In the framework of the EMACOP project, the behaviour of the device in front of a dike is modelled, as shown by the 2D sketch in Fig. 1. The water depth of 11.5m and 10m used for the numerical simulations

corresponds respectively to Bayonne and Saint Jean de Luz site bathymetry and justifies the use of two distinct flap geometries.

TABLE I
MAIN CHARACTERISTIC OF THE PITCHING FLAP

Characteristics	Unit	Bayonne site	Saint Jean de Luz site
Flap width	m	20	20
Flap thickness	m	1.5	1.5
Mass of steel (flap only)	tons	67.8	60
Pivot axis	m	-9.5	-8
CG (z-coord.)	m	-3.2	-2.7
Base height	m	2	2

B. Implantation configurations of the WEC in front of a dike

1) Case-study for power matrix assessment

The power matrix assessment is based on a 3D BEM approach and choice has been made to model the dike with symmetry considerations (see §II.A.2). For that reason, at this stage of our study, the power matrix assessment has been made for a pitching flap placed in front of a fully reflecting vertical dike, as shown in Fig. 1. Two distances between the flap and the dike are considered here: 15m and 30m.

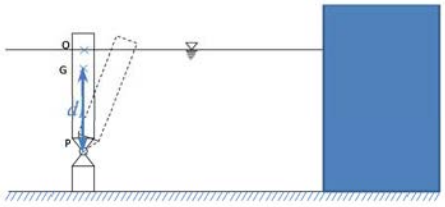

Fig. 1 Pitching flap in front of a vertical dike

2) Case-study for extreme loads estimation

For the extreme loads estimation, based on an SPH approach (see §IV), the actual configuration of wall inclination of Bayonne's dike has been used. A distance of 15m between the flap and the dike has been considered.

3) Wave resource

In both BEM and SPH numerical models, the direction of incident waves is supposed to be normal to the dike. The scatter diagram of the wave statistics used to evaluate the mean power absorbed on Saint Jean de Luz and Bayonne [3] sites are presented in Fig. 2. To establish this scatter diagram, wave data are issued from the ANEMOC database [4] for an offshore location, and propagated nearshore using Goda's analytical formula [16].

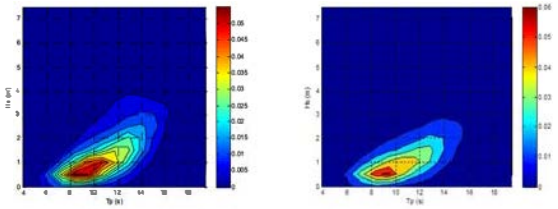

Fig. 2 Bayonne and Saint Jean de Luz scatter diagram

JONSWAP spectra with a γ=3.3 frequency spreading parameter is used to model irregular sea states, and the water detph corresponding to half tide depth is used for both site. The mean annual wave resource estimated from Eq.1 is 21.8kW/m at Bayonne site, and 16.6kW/m at Saint Jean de Luz site.

$$P = \rho g \int_0^\infty C_g(f) S(f) df \quad (1)$$

ρ is the water density, g the gravity, $C_g(f)$ the group velocity of the waves, $S(f)$ the wave spectrum.

The influence of tides on the absorbed power is neglected in this paper. It is currently being assessed in a further study.

III. POWER MATRIX ASSESSMENT

The time domain wave to wire model developed here is based on the integration of the motion equation of the WEC described hereafter. The aim is to compute the power matrix. The product of this power matrix by the Bayonne or Saint Jean de Luz scatter diagram enables with the evaluation of the mean annual absorbed power at those locations [1].

A. Methodology

The specificity of the study lies in the modelling of the vertical dike by means of symmetry considerations. Let's, first of all, establish the equation of motion for an isolated flap [7]:

1) Equation of motion of the isolated flap

The forces which govern the flap dynamics, and associated assumptions are the following:

- *Wave-structure interactions:*

Linear potential flow theory is used to model waves as well as wave-structure interactions. Therefore, the usual assumptions of incompressible and inviscid fluid, irrotational flow, small amplitudes of motion relative to the device dimension and small wave steepness are made. In frequency domain, the hydrodynamic radiation coefficients $C_M(\omega), C_A(\omega)$ as well as the wave excitation torque τ_{ex} have been calculated using the 3D Boundary Element Method Aquaplus code [5]. The mesh convergence was checked, the pressure force resulting from wave-structure interactions can therefore be expressed as :

$$\tau_{WS} = \tau_{ex} - C_M(\omega)\ddot{\theta} - C_A(\omega)\dot{\theta} \quad (2)$$

$\dot{\theta}$ and $\ddot{\theta}$ being respectively the angular velocity and acceleration of the flap

- *Hydrostatic force*

The hydrostatic torque on the flap is expressed as $\tau_H = -C\theta$, where θ is the rotation angle of the flap, and:

$$C = K_{55} + g(\rho V - M)d_1 - M_{PTO}gd \quad (3)$$

- K_{55} being the hydrostatic stiffness of the flap if it would be neutrally buoyant [1]
- The second term is the product of the net buoyancy by the vertical distance from hinge to centre of gravity of the flap
- The third term the product of a ballast weight M_{PTO} by the vertical height

- *Viscous effects*

Considering our partly submerged pitching flap, it is expected that usual assumptions of linear potential flow theory such as linearity and irrotationality will not be valid in all wave conditions. A simplified approach used to model viscous effects such as flow separation consists in adding a quadratic damping term in the equation of motion, similar to the drag term in Morison's equation [6]:

$$F_{vsc} = -\frac{1}{2}\rho C_d S_d (V - V_0)\|V - V_0\| \quad (4)$$

Where :

- C_d and S_d are respectively the drag coefficients and characteristic areas
- V and V_0 are respectively the device velocity and undisturbed flow velocity

The viscous torque on the flap is therefore estimated by dividing the flap into ten horizontal sections and computing the viscous force F_{vsc} on each section.

- *Power Take Off*

A linear PTO model is applied here; the PTO torque being decomposed into 3 terms (Eq.5) :

- A linear damping term proportional to the velocity of the flap; B_{PTO} being the damping coefficient
- A spring-like term; K_{PTO} being the machinery spring coefficient.
- An inertia term may be used to tune the dynamic response of the flap. To this end, the flap can be water ballasted in order to increase its inertia.

$$\tau_{PTO} = -M_{PTO}\ddot{\theta} - B_{PTO}\dot{\theta} - K_{PTO}\theta \quad (5)$$

- *Equation of motion*

Given those assumptions and force definitions, by expressing Newton's law at point P of the hinge, one can write the equation of motion of the flap in the frequency domain :

$$\left(M_{55} + C_M(\omega)\right)\ddot{\theta} = -C_A(\omega)\dot{\theta} + \tau_{ex} + \tau_H + \tau_{PTO} \quad (6)$$

With $M_{55} = I_y + (Md_1^2 + M_{PTO}d^2)$: the inertia of the flap

The corresponding equation of motion of the isolated flap in the time domain is the following:

$$(M_{55} + \mu_\infty)\ddot{\theta} = -\int_0^t K_{rad}(t-\tau)\dot{\theta}(\tau)d\tau + \tau_{exc} + \tau_H + \tau_{PTO} + \tau_{vsc} \quad (7)$$

Where : $\mu_\infty, K_{rad}(t), \tau_{exc}(t)$ are respectively the added mass, the memory function of the radiation forces and the excitation torque, calculated from :

$$\mu_\infty = \lim_{\omega\to\infty} C_M(\omega) \qquad K_{rad}(t) = \frac{2}{\pi}\int_0^\infty C_A(\omega)\cos(\omega t)\,d\omega$$

$$\tau_{exc}(t) = a\Im(\tau_{ex}(\omega)e^{-i\omega t}) \quad (8)$$

The response of the flap to an irregular sea state will then be determined using the superposition principle:

$$F_{ex}(t) = \sum_i\left(\sqrt{2S(f_i)\Delta f}\right)F_{ex}(f_i)e^{-i(2\pi f_i t + \phi_i)} \quad (9)$$

$S(f)$ being the incident wave spectrum, Δf being the frequency step, ϕ_i : a set of random phases

Once described the equation of motion of the isolated flap (Eq.7), the principle of dike modelling using symmetry considerations is explained in order to form the equation of motion of the global {flap + dike} system.

2) Dike modelling principle

The dike is considered to be a fully reflecting vertical wall and is modelled using symmetry consideration by adding a second flap at twice the distance to the dike (Fig. 3) with a motion opposed to that of the first flap.

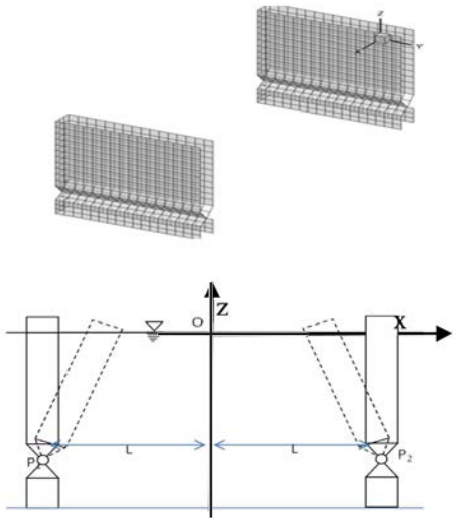

Fig. 3 : Mesh used for the Aquaplus calculation (on top), Dike modelling principle

The symmetrisation of the problem leads us to consider the superposition of 2 waves; one propagating towards positive x, the other towards negative x.

Concerning wave excitation force, we look for amplitudes and phase conditions for the potential to obtain a wall condition at the dike. Considering a dike positioned on x=0, and a phase origin x=-L (i.e. flap1 location), we look for conditions so that $V_x^+ + V_x^- = 0$ for x=0;

For the incident wave potentials, writing both potentials for wave propagating along positive x and negative x (Eq.10), we find out that, to satisfy watertightness criterion $\frac{\partial\phi_I^+}{\partial x} + \frac{\partial\phi_I^-}{\partial x} = 0$ for x=0, we must have $A^+=A^-$ and $\Psi^- = 2kL$.

$$\phi_I^+(x,z,t) = \frac{A^+ g}{\omega}\frac{\cosh(z+h)}{\cosh kh}\sin(k(x+L) - \omega t)$$

$$\phi_I^-(x,z,t) = \frac{A^- g}{\omega}\frac{\cosh(z+h)}{\cosh kh}\sin(-k(x+L) - \omega t + \Psi^-) \quad (10)$$

For the diffracted wave potential; ϕ_I^+ and ϕ_I^- being symmetrical, diffraction problems are also symmetrical. It leads to $\frac{\partial\phi_D^+}{\partial x} + \frac{\partial\phi_D^-}{\partial x} = 0$ for x=0.

When placed in front of a vertical dike, the excitation force seen by the flap will be: $\tau_{ex}^{bw} = \tau_{ex1}^+ + \tau_{ex1}^- e^{2ikL}$ (11)

τ_{ex1}^{+} being the excitation torque on the first flap(x=-L) for a wave propagating towards x positive

$\tau_{ex1}^{-}e^{2ikL}$ being the excitation torque on the first flap (x=-L) for a wave propagating towards x negative

Finally, when placed in front of a vertical dike, the hydrodynamic forces expressed here in frequency domain applied on the flap are:

$$\tau_{WS}^{bw}(P) = \tau_{ex}^{bw}(P) - (CM_{1155} - CM_{1255})\ddot{\theta} - (CA_{1155} - CA_{1255})\dot{\theta} \quad (12)$$

CM_{1155} and CM_{1255} are the radiation coefficient corresponding to an effort on flap 1 associated with the pitch motion of flap 1 and with the pitch motion of flap 2 (respectively CA_{1155} and CA_{1255}).

3) Equation of motion of the flap in front of a vertical dike:

The equation of motion of the flap in front of a vertical dike in frequency domain is therefore obtained by applying Newton's law at point P of the hinge of the flap :

$$\left(I_y + (M + M_{PTO})d_1^2 + (CM_{1155} - CM_{1255})\right)\ddot{\theta} + \left((CA_{1155} - CA_{1255}) + B_{PTO}\right)\dot{\theta} + (K_{55} + g(\rho V - M - M_{PTO})d_1 + K_{PTO})\theta = \tau_{ex1}^{+} + \tau_{ex1}^{-}e^{2ikL} \quad (13)$$

In time domain, the equivalent equation of motion is obtained, adding the viscous effects τ_{Visc}, similarly to equation 7, and using definitions of equation 8.

B. Numerical implementation and code verification

Both frequency and time domain Wave to Wire models have been implemented in FORTRAN. This twin implementation enabled to validate the numerical developments through comparison of RAO as shown on Fig. 4 where we can notice that frequency and time domain RAO computations are identical.

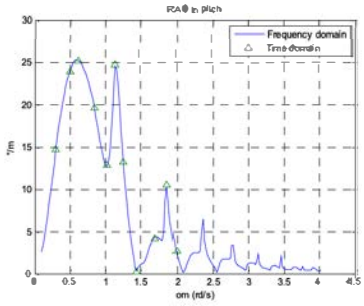

Fig. 4 Pitch RAO of the flap placed 15m in front of the dike, B_{pto}=3.4E7Nsrd^{-1}, K_{pto}=0; 10m depth configuration

Considering here the configuration of the flap in front of a dike, one can note that RAO, as well as power functions (Fig. 5) and excitation torque (Fig. 7) exhibit minima at specific frequencies directly linked to the position of nodes and antinodes of the standing wave field developed in front of a fully reflecting vertical wall.

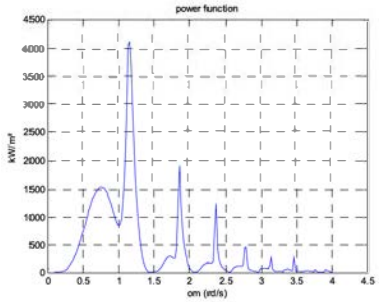

Fig. 5: power function (kW/m²) of the flap placed 15m in front of the dike, B_{pto}=3.4E7Nsrd^{-1}, K_{pto}=0; 10m depth configuration

Analytical developments [2] for a similar system showed that minima of the excitation torque occur for = $m\pi$, m=1,2,..., k being the wave number, d the distance to the dike. The position of those minima corresponds to the antinodes position (Fig. 6) of the standing wave developed in front of the dike and is also well predicted by our numerical model (Fig. 7). The minima correspond to locations where the velocity of the particles is purely vertical.

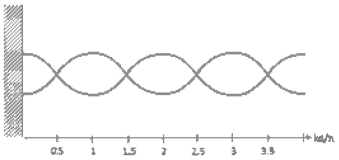

Fig. 6: Illustration of the standing wave field developed in front of a vertical dike

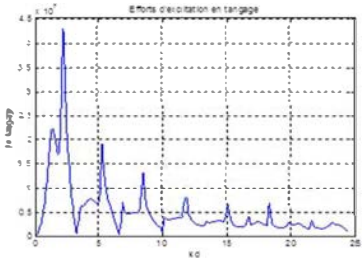

Fig. 7 Excitation torque on the flap placed 15m in front of the dike, 10m depth configuration

On the other hand, the peak of the excitation torque and power function occurs near the nodes of the standing wave field, near $kd = (m + 1/2)\pi$ locations, where the motion of the particles at the nodes is purely horizontal.

C. Power matrix assessment and associated uncertainties

1) Power matrix assessment

JONSWAP spectra have been used to simulate irregular sea states. The power matrix of the flap located in front of a vertical dike was determined simulating the behaviour of the device for each one of the sea states. An optimisation loop was implemented in order to optimise B_{PTO} and K_{PTO} coefficients for each sea state. Due to simulation durations, power matrix assessment has been made using the frequency domain model (thus without taking into account viscous effects). The results of the simulations are illustrated in Fig. 8

for a 10m depth site; the flap being placed 15m in front of the dike.

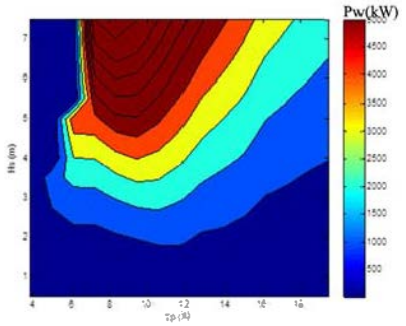

Fig. 8 Power matrix of the flap placed 15m in front of the dike, 10m depth configuration

2) Viscous effects analysis and associated uncertainties

The analysis of viscous effects on a flap located in front of a dike will enable the estimation of viscous losses and associated impacts on absorbed power. For the current computations, the drag coefficient is taken from literature [7]; a dedicated study based on a CFD approach is currently being performed in order to compute the drag coefficient for our flap configuration. In irregular sea states, few simulations have been performed up to now. For example, considering an irregular sea state with a 9.6s peak period, the absorbed power reduction is about 44% for a $H_s=2m$ wave, and about 20% for a $H_s=1m$ wave. Babarit et al [7] had evaluated a 30% power reduction due to viscous effects on a similar bottom mounted flap in an isolated configuration. Further investigation should be performed in order to evaluate accurately the power reduction in all sea states of a given scatter diagram; this study will have to include an optimisation process of the PTO parameters for each one of the sea states.

3) Mean annual power estimation

Taking benefit of the reflections on the dike, and without taking into account viscous effects, the estimated capture width ratio for a flap placed 15m in front of the dike in Saint Jean de Luz site is about 156%. Table 2 shows the evaluation of mean absorbed power for different configurations of the flap taking into account a 40% reduction due to viscous effects (Pw_1). For Saint Jean de Luz site, the capture width ratio is more than doubled between the configuration of the isolated flap (46%) and the flap placed 15m in front of a vertical dike (96%). Finally, estimating a global 70% efficiency for the power take-off system (for all the sea states), and taking into account the effect of viscous losses, the estimated mean available electrical power of a flap placed 15m in front of a dike is therefore 220kW in Saint Jean de Luz site, and 260 kW in Bayonne site (see Table II) .

TABLE II
MEAN ANNUAL POWER, AND CAPTURE WIDTH RATIO OF THE FLAP

		Isolated Flap	Flap - dike 15m	Wave (kW/m)
Saint Jean de Luz	Pw_1 (kW)	150	320	16,5
	η (%)	46	95	
	Pw_2 élec (kW)	105	220	
Bayonne	Pw (kW)	-	370	22
	η (%)	-	85	
	Pw2 élec (kW)		260	

A computation of the power matrix has also been made for the case of a flap located 30m in front of a dike, for Saint Jean de Luz site configuration. The estimated absorbed power is therefore P_{w1}=350kW, which is 9% greater than in the case of a flap placed 15m in front of the dike, and confirms, as already stated in §B analysis in the case of regular waves, the influence of the distance flap-dike on the flap behaviour. If we consider wave periods from 10s to 16s (that represent 62% of the waves in Saint Jean de Luz), the location of the first node of those waves is between 23m and 38m from the dike. Compared with the configuration of a flap 15m in front of the dike, being 30m away from the dike, the flap is therefore nearer from a node of the standing wave field developed in front of the dike if we consider the most frequent wave periods of Saint Jean de Luz site : this may explain the increase of absorbed power.

The results obtained here show that in the case of a partly submerged pitching flap, we can really take benefit from the reflection of waves on the dike: As mentioned here above, power absorption might be doubled compared with an isolated flap configuration. Due to the development of a standing wave field in front of a fully reflecting vertical dike in regular sea states, the distance to the dike has great influence on the flap behaviour, and according to the results of §B., the flap should not be placed near an antinode of the standing wave field.
The main uncertainties in the assessment of mean annual absorbed power remain the estimation of the viscous effects, the efficiency of the PTO, and the applicability of a theoretical 'pure' reflector to model the dike. Concerning the estimation of the viscous effects, from early calculations (§C.II), the estimation made here is a reduction of about 40% of the absorbed power due to viscous effects. Further studies should be performed, in order to evaluate more accurately losses due to viscous effects. Another point neglected here, due to time consuming computations, is the influence of the tide on the performances of the device. This parameter is also currently being studied.

4) Performance criteria

The evaluation of the absorbed power is essential in the process of analysis of a given WEC, but only performance measures will be related to costs and will enable to compare WECs performances [1]. Therefore, as a first approach, the energy per characteristic mass as well as energy per characteristic surface area is evaluated. The results are

compared to those of a 5m radius heaving buoy placed 10m in front of a dike, also studied in the framework of the EMACOP project [8]. The characteristic mass and surface area are directly extrapolated from the bottom-hinged flap data evaluated by Babarit et al [1]. Fig. 9 show better performances of the flap for both the 'isolated' and 'coupled with a dike' configurations compared with the heaving buoy for both sites. The same results had already been highlighted by Babarit et al.[1] for equivalent WEC devices considered in the 'isolated' configuration. Fig. 9 shows the performance gain – here a factor of 2- obtained in the case of coupling with the dike compared with the isolated configuration for both devices. However, this gain has to be moderated, reminding that the dike is here considered to be a fully reflecting wall (where a real vertical dike would exhibit a 0.75 maximum reflection factor) submitted to normal incident waves, without taking into account any tidal effect.

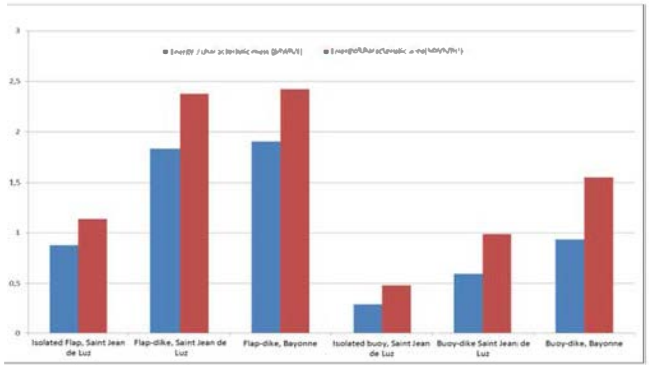

Fig. 9 Performance criteria of the flap compared with those of a heaving buoy : in blue : energy per characteristic mass, in red : energy per surface area.

IV. EXTREME LOADS ESTIMATION

A. SPH modelling

Both compressible and incompressible formulations of SPH can be encountered in the literature. We focus here on its compressible form, used to model weakly-compressible fluids. The theoretical scheme used by the SPH model is briefly summarised. Since the Reynolds number of the considered flow is quite high, viscous effects can be considered negligible. Therefore, the fluid being treated as weakly-compressible, the continuity equation for compressible fluids is used together with the Euler equation:

$$\begin{cases} \dfrac{D\rho}{Dt} + \rho \nabla \cdot \mathbf{u} = 0 \\ \rho \dfrac{D\mathbf{u}}{Dt} = -\nabla p + \rho \mathbf{g} \\ \dfrac{D\mathbf{r}}{Dt} = \mathbf{u} \end{cases}$$

where D/Dt represents the Lagrangian derivative, while $\mathbf{r}$, $\mathbf{u}$, p and ρ are, respectively, the position of a generic material point, its velocity, pressure and density; $\mathbf{g}$ represents the gravity acceleration. Moreover, the fluid is assumed to be barotropic and, therefore, the following functional dependence between ρ and p is adopted:

$$p(\rho) = \frac{c_0^2 \rho_0}{\gamma} \left[\left(\frac{\rho}{\rho_0} \right)^{\gamma} - 1 \right] + p_0$$

where ρ_0 and p_0 are constant, c_0 is the sound speed and γ is a dimensionless parameter greater than 1 (in all the following examples $\gamma = 7$ is used). The sound speed c_0 is chosen as small as possible to ensure $Ma < 0.1$, since the acoustic part of the solution is not of interest in the present context, even if locally compressible effects can matter during violent impact events [11]. Furthermore, in order to reduce the computational costs, only the liquid phase is modelled.

The system is written in a Lagrangian way, which stands for one of the main interest of this particle method. The fluid domain is therefore discretised in a set of particles, each particle settling with the fluid velocity and carrying its own flow quantities (mass, pressure, etc.).

The results shown in the following have been obtained through the "SPH-Flow" solver, a software co-developed by Ecole Centrale de Nantes and HydrOcean company. For further details on the specific implementation here adopted, the reader is referred to [9] and [14].

B. Methodology

Very few works are present in the literature addressing the numerical study of extreme sea loads on coastal moving flaps. Moreover, to the authors' knowledge only two works have addressed the SPH simulation of this kind of devices (see [10] and [12]). Anyhow, no study focused on extreme loads has been performed in those works. In order to tackle the problem of the deterministic assessment of the extreme loads on the flap-type energy converter the most critical wave conditions have to be defined. Two unknowns combine in the definition of this scenario: on one side the actual shape of the extreme wave at the impact stage; on the other side the configuration of the flap (i.e. rotation angle and angular velocity) at the same instant, that results from its previous time history.

In a first approximation the wave is generated directly by the SPH solver through a numerical wavemaker. The characteristics of the extreme wave to be generated are defined through semi-empirical formulae as described in the following. The wavemaker velocity law is thus derived in order to reproduce such wave in a numerical tank. The present analysis can, therefore, give useful indications for the design of the structure but, due to large approximations underlying the wave generation, represents only a qualitative evaluation of the loads acting on the structure.

All the simulations are firstly run in the 2D framework. The wave is generated firstly in a large numerical basin without the presence of the flap and breakwater in order to make easier the generation of the design wave. The wave parameters are slightly tuned in order to obtain the steepest wave possible in a given range of wave heights and periods. Then, the fluid domain of the fully developed wave is used as initial condition for wave impact simulations.

Then, the numerical tank is cut by adding the flap and the breakwater. A test case matrix is defined (see table 3) by varying the depth and the distance of the flap from the wave in order to investigate the dependence of the impact loads on, respectively, the tide level and the wave shape at the impact. In fact, during its propagation the wave evolves and breaks due to the large steepness and the loads on the structure are

strictly related to the flap configuration with respect to the breaking process (see e.g. [13], [14], [15]). Moreover, an additional non-linearity is due to the fact that the flap interacts with the flow before the actual impact, being free to rotate according to the hydrodynamics forces.

It is worth noting that the depth is a critical parameter in the calculations. Indeed, the maximum tidal range is about 4.4 m and the impact evolution turned out to be largely dependent on the mean water level. Therefore a large range of water depths is tested in order to assess its influence. The simulations where the most critical loads take place have been selected to be reproduced in the 3D framework. In the latter case, since large computational resources are required, a multi-resolution approach is adopted, verifying the differences with respect to the 2D case.

C. *Numerical setup*

For the generation of the wave the adopted numerical setup is composed by the piston wavemaker inside a tank long enough to avoid reflections or influences of the boundaries. Neither the flap energy converter nor the breakwater are present in this preliminary simulation. The characteristics of the design wave, in terms of period and wave height, were computed starting from the data recorded at the buoy closest to the Bayonne site. Given a certain couple of period and wave height, through the Goda's formula [16] the corresponding values of the highest breaking wave close to the shore can be inferred. In this way several couples of periods and wave heights were tested in the numerical wave tank in order to find the steepest wave. To this aim a sinusoidal motion law has been prescribed to the piston wavemaker following the formulae described in [17]. Finally, the couple (T;H) = (15.0 s; 10.39 m) has been found to be the most critical. Given the large steepness, the wave breaks in a large plunging jet. However, the simulation is stopped before the actual breaking and the obtained particle configuration is used inside a shorter tank limited by the flap in front of the dike (see sketch in bottom plot of Fig. 10). In Fig. 10 the adopted numerical setup is shown (note that the distance of the flap from the wavemaker, x_{flap}, and the water depth are not fixed as reported in Fig. 10). For the sake of completeness, a view of numerical domain adopted for the 3D simulation is provided in Fig. 11. In the latter case the tank width has been chosen equal to 60 m in order to avoid possible reflections from the lateral walls. Note that in the 2D case the hinge is detached from the bottom to allow the fluid flowing under the flap.

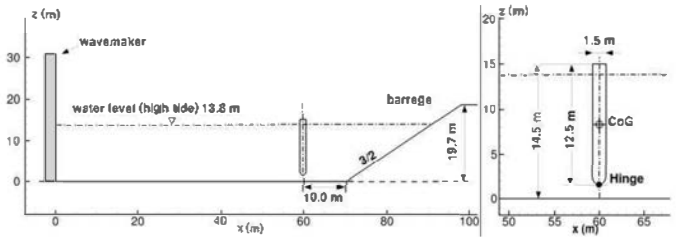

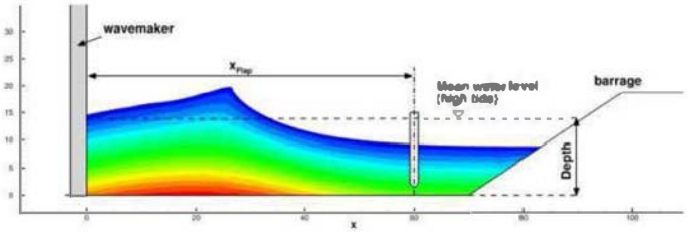

Fig. 10 Geometrical configuration adopted for the 2D and 3D simulation.

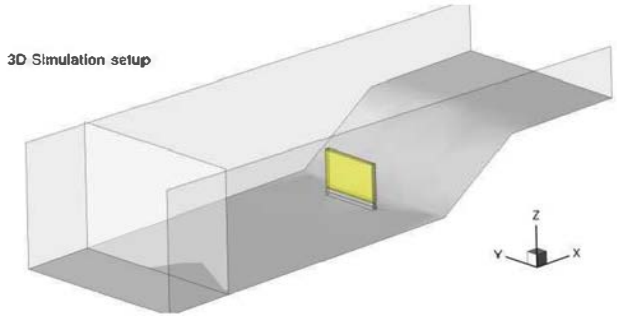

Fig. 11 view of 3D numerical setup

The mean particle spacing adopted is the same for all the simulations and is equal to x = 0.1 m. The simulation time has been chosen long enough to allow the full impact development and is about 10 s.

TABLE III
TEST CASE MATRIX OF THE 2D SIMULATIONS

Label	Water Depth (m)	X_{flap} (m)
HT50	13.8	50
HT60	13.8	60
HT80	13.8	80
HT100	13.8	100
MT50	11.3	50
MT60	11.3	60
MT80	11.3	80
MT100	11.3	100
BT50	8.8	50
BT60	8.8	60
BT80	8.8	80
BT100	8.8	100

Note that the presence of the flap and/or the variation of the depth can induce a different evolution of the wave compared to the simulation of the wave alone travelling in the void tank. However, the propagation time before the impacts are quite small and, therefore, no remarkable modifications occur on the wave height and length. On the other hand, because of the large steepness of the incoming wave the breaking occurrence is more sensible to these changes (the wave being close to its stability limit).

D. *2D Numerical results*

Quite different impact dynamics are obtained depending on the wave shape at the impact instant. In most of the test cases the maximum values of the force and torque are around 0.5 MN and 1 MN·m respectively. However, in some cases much larger values are recorded. For the sake of conciseness only the plots related to water depths equal to 11.3 m (MT series)

are shown. In Fig. 12 and Fig. 13 the global loads recorded on the flap in terms of horizontal force and torque around the hinge are reported. For values of the parameter $x_{flap} \leq 80$ m the load histories are similar, though delayed.

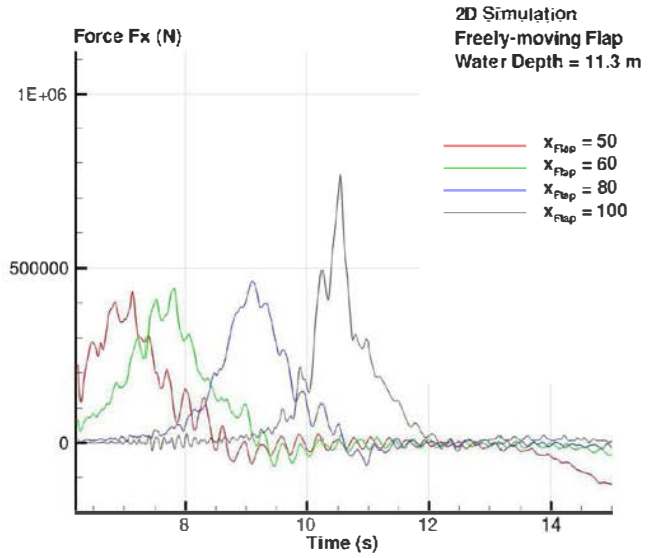

Fig. 12: Global loads acting on the flap in terms of horizontal force for mean water depth equal to 11.3 m.

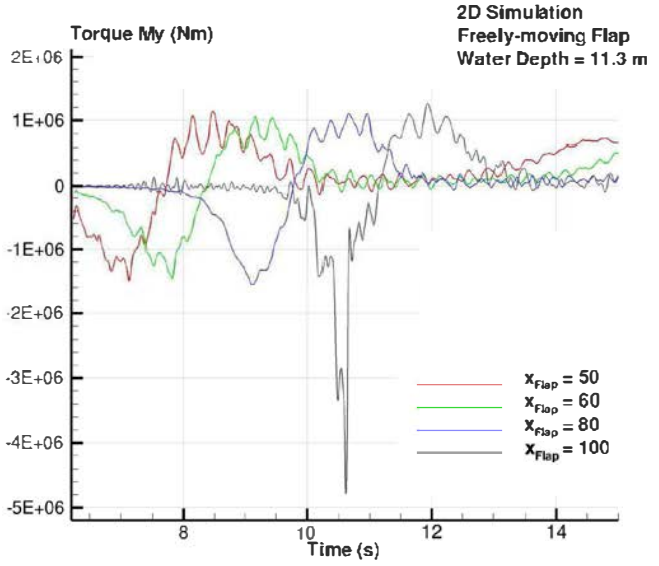

Fig. 13 Global loads acting on the flap in terms of torque around the hinge for mean water depth equal to 11.3 m.

Conversely, for x_{flap} = 100 m, and also for the cases BT80 and BT100, a quite different evolution is recorded. This is due to the fact that the impact dynamics is rather different in latter case. When the distance between the wave and the flap is not large enough the impact occurs before the breaking inception and, therefore, the resulting load is rather weak. This is the case for the vast majority of the considered simulations. For instance in two instants of the impact stage are shown for the case MT80. In this case since the wave approaches the flap with a gentle slope the pressures remain generally of the same order of the hydrostatic ones.

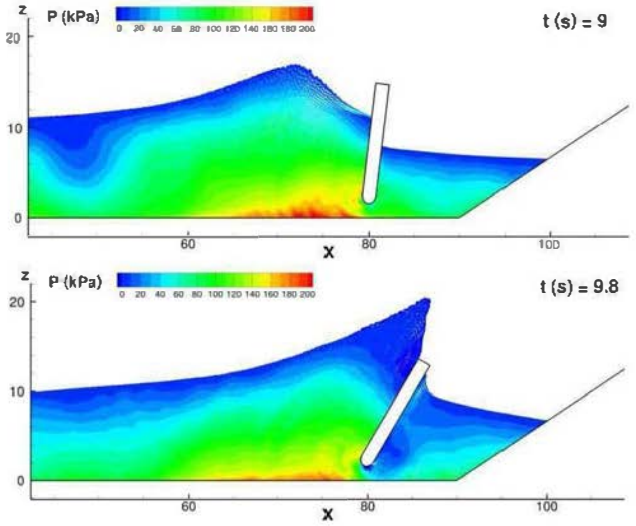

Fig. 14 Flow evolution around the impact instant for the case MT80

Conversely, in the cases MT100, BT80 and BT100 the impact occurs at the breaking inception. As shown in Fig. 15, the wave front approaches the flap with a rather steep front and the occurrence of a flip-through behavior is well visible (see e.g. [18]). In this case the impact is characterized by very small time and space scales. This behavior can be better observed in Fig. 16 where the pressure measured along the flap is plotted on the time-space plane.

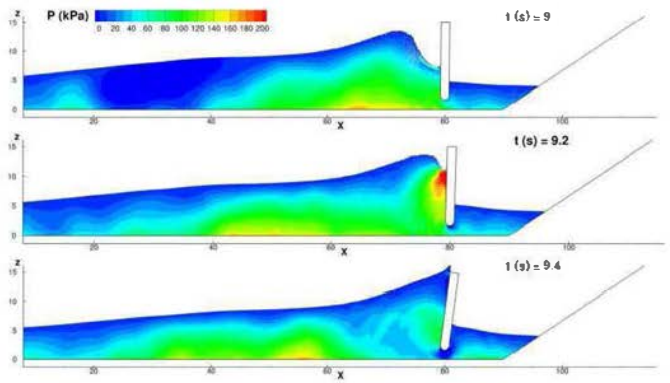

Fig. 15 Flow evolution around the impact instant for the case BT80.

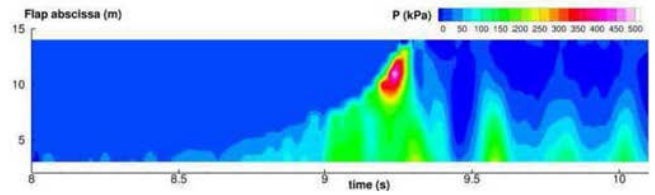

Fig. 16 Evolution of the measured pressure on the flap in the time-space plane for the case BT80.

A pressure peak close to 500 kPa is observed around t=9:25 s. This pressure increase expires in few tenths of seconds and involves a space scale of about 0.1 m. The sudden increase in

the pressure is also due to the fact that, differently from the case in, at the impact instant the flap is only just starting to move (Fig. 14), because of the steeper shape of the wave. Therefore, the momentum transfer from the wave to the flap takes place in a much shorter time interval, thus resulting in a further contribution to the load on the structure.

E. 3D Results

On the base of the 2D results the test cases MT100 and BT80 have been selected to be replicated in the 3D model. The same procedure as the 2D case has been followed: the wave has been firstly generated in a void tank and then the flap and the breakwater have been added. However, in order to reduce the CPU costs, this time a varying particle resolution model has been employed. The minimum particle size $\Delta x = 0.1$ m is maintained only in the neighborhood of the flap position. The particle size is then gradually enlarged both on the x and y directions. Note that the barycenter of the fine resolution region is around $x = 70$ m (Fig. 17) in order to have a higher resolution on the wave front at impact instant. The effect on the solution of the multi resolution scheme has been checked and a comparison of the obtained wave profile between 2D and 3D model is shown in Fig. 18. The two solutions are practically overlapping. Both the 3D simulations MT100 and BT80 involved about 10 million particles and ran on 200 cores for about 48 hours.

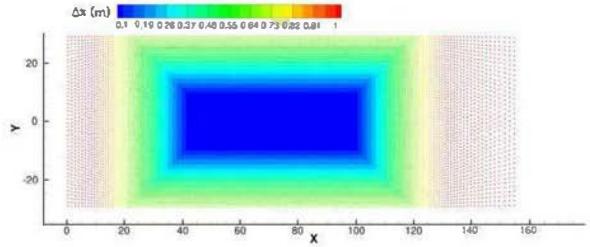

Fig. 17 top view of the 3D initial particle configuration: the highest resolution ($\Delta x = 0.1$ m) is adopted only in the region close to the flap.

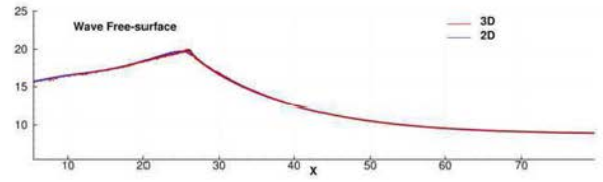

Fig. 18 comparison of the wave profile obtained through the 2D and 3D models.

In Fig. 19 and Fig. 20 the free-surface evolution is depicted with two different angle of view before and after the impact. Differently from the 2D cases, here the breaking starts before the impact. Notwithstanding that, the wave impacts the flap with a quite large front steepness causing a complex 3D splashing with several jet ejections and fragmentations. Similar to figure Fig. 16 at the impact stage the flap rotation is still very small. In Fig. 21, the pressure field on the flap face at time $t = 9.3$ s is reported. With respect to the 2D simulation of Fig. 15 and Fig. 16 here the field is less smooth due to fragmented wave front. However, the pressure peaks are close to the 2D case although more scattered in space and time during the impact. As for the global loads the time history of the torque around the hinge is reported in Fig. 22 along with the evolution predicted by the 2D model (amplified to take into account the flap width). The latter overestimates the peak by a factor close to 2.0. This can be justified by two reasons: firstly the wave impact occurs in a larger time interval (due to the non-uniform shape of the front); secondly the flap has a shape close to square and, therefore, 3D effects on the entire flow can be non-negligible. Similar conclusions are drawn also for the case MT100.

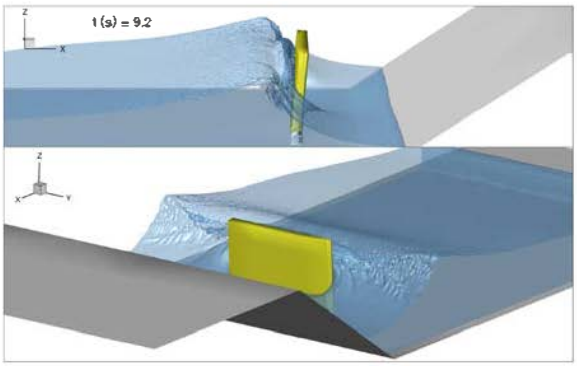

Fig. 19 Free-surface evolution of the 3D case BT80 before the impact at t=9.2 s. Top plot: side view. Bottom plot: angular view.

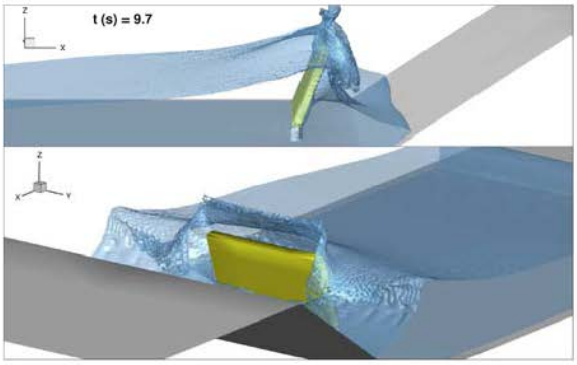

Fig. 20 Free-surface evolution of the 3D case BT80 before the impact at t=9.7 s. Top plot: side view. Bottom plot: angular view.

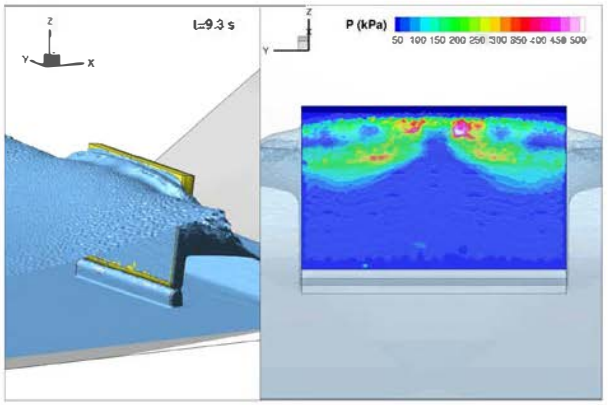

Fig. 21 Free-surface (left) and pressure field on the flap (right) of the 3D case BT80 at time t=9.3 s. Top plot: side view. Bottom plot: angular view..

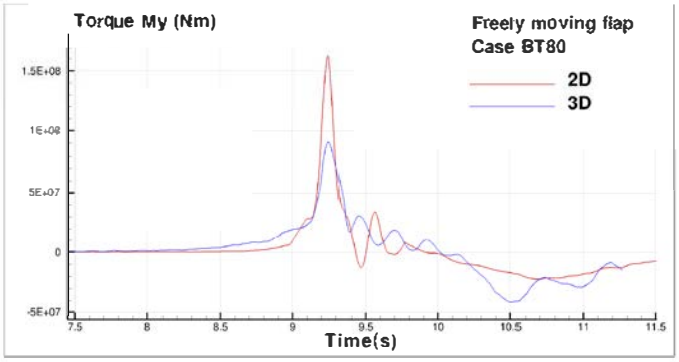

Fig.22 comparison of the torque around the hinge evaluated by the 2D and 3D models

V. CONCLUSION

A complementary use of a potential code and SPH code enabled to assess both power matrix and extreme loads on a partly submerged pitching flap placed in front of a dike.

The use of a potential code and associated good performances in terms of calculation speed enabled to assess numerically the power matrix and permitted the computation of the yearly mean absorbed power in Saint Jean de Luz and Bayonne site.

The specificity of the paper concerns the simulation of a WEC coupled to a dike. Symmetry considerations are used to model an idealised fully reflecting vertical dike. The analysis showed that, for specific frequencies such that $kd=m\pi$ which corresponds to the antinodes of a standing wave field that developed in front of the dike in regular sea states, extinctions in the excitation torque occur. To take benefit from the reflections on the dike, the flap should therefore be placed away from those specific locations. Results here showed that, for a flap situated 15m in front of a fully reflecting vertical dike, in the specific site of Saint Jean de Luz or Bayonne, the capture factor may be increased by a factor 2 compared with an isolated flap. However, this gain has to be moderated because it has been obtained in the configuration of a fully reflecting wall, where a real vertical dike would exhibit a maximum reflection factor of 0.75. Moreover, further investigations will have to be performed in order to evaluate more precisely the effects of viscosity. Regarding extreme loads estimation on the flap using SPH modelling, an in-depth analysis of the extreme loads acting on a flap energy converter in both 2D and 3D frameworks has been performed using a SPH numerical solver. In a first approximation, the highest possible breaking wave to shore was estimated from recorded wave data at a buoy close to Bayonne site and propagated to shore via Goda's formulae. A sinusoidal motion corresponding to that steep wave is then prescribed to the numerical piston wavemaker, directly within the SPH solver. The dependence of impacts loads on tide levels and wave shape at the impact have been investigated. For the most critical impact case, when the impact occurs at the breaking inception, 3D SPH computations have been performed, and 3D effects have been highlighted through the comparison of time history of the torque around the hinge in both 2D and 3D frameworks.

ACKNOWLEDGMENT

Financial support by the French EMACOP project and LabexMer (grant ANR-10-LABX-19-01) is acknowledged. The SPH simulations performed in the frame of the present research have been obtained through the "SPH-Flow" solver, a software co-developed by Ecole Centrale de Nantes and HydrOcean company.

REFERENCES

[1] Babarit A., Hals J., Muliawan M.J., Kurniawan A., Moan T., Krokstad J. (2011). Numerical benchmarking study of a selection of wave energy converters, Ren. Energy, 41

[2] Sarkar D., Renzi E., Dias F. – wave power absorption from a flat-type Wave Energy Converter near a straight coast – Proceedings of 9th European Wave and Tidal Energy Conference 2013, Aalborg , Denmark, 2-5 september 2013

[3] E.Cosquer, G.Dufour, B.Michard – Evaluation préliminaire du potentiel houlomoteur de 22 sites français en Manche et Atlantique – Study report CETMEF-EGIS, EMACOP project

[4] http://anemoc.cetmef.developpement-durable.gouv.fr/)

[5] Delhommeau G. Seakeeping codes aquadyn and aquaplus. In: Proc. of the 19th WEGEMT school, numerical simulation of hydrodynamics: ships and offshore structures; 1993.

[6] Molin B. : Hydrodynamique des structures offshore,, Editions Technip , 2002

[7] Babarit A., Hals J, Kurniawan A., Muliawan M., Moan T. and Krokstad J., Numerical estimation of energy delivery from a selection of wave energy converters, NumWEC project final report

[8] Baudry V, Babarit A, Clément AH, Développement d'un outil d'évaluation du rendement des dispositifs houlomoteurs de type flotteur pilonnant, EMACOP project

[9] Oger, G., Guilcher, P. M., Jacquin, E., Brosset, L., Deuff, J. B., & Le Touzé, D. (2010). Simulations of hydro-elastic impacts using a parallel SPH model. *International Journal of Offshore and Polar Engineering*, *20*(3), 181-189

[10] Rafiée A., Dias F., Numerical simulation of wave impact on an oscillating wave surge converter, 2nd Int' conference on Violent Flows, Nantes, France, September 25-27, 2012

[11] Korobkin, A., Pukhnachov, V., (1988). Initial stage of water impact. *Annual Review of Fluid Mechanics 20*, 159–185.

[12] Chen D.-W., Tzang S.-Y., Hsieh C.-M., Chow Y.-C., Chen J.-H., Lin C.-C., and Hwang R. R.-J (2014). Numerical Modeling of Wave-induced Rotations of a Bottom-hinged Flapper with a SPH Model. *Journal of Marine Science and Technology, 22*(3), 372-380.

[13] Kimmoun O., Ratouis A., and Brosset L., Sloshing and scaling: experimental study in a wave canal at two different scales. *Proceedings of 20th International Offshore and Polar Engineering Conference*, June 2010, pp. 20–26.

[14] Guilcher P.M., Jus Y., Couty N., Brosset L., Scolan Y.M., Touzé D. Le, et al., 2D Simulations of Breaking Wave Impacts on a Flat Rigid Wall - Part I: Influence of the Wave Shape. *In Proc. 24th Int. Ocean and Polar Eng. Conf., ISOPE*, Busan, 2014.

[15] Lu X. Z., Cherfils J-M., Pinon G., Rivoalen E., and Brossard J., SPH Numerical computations of wave impact onto a vertical wall. *In 9th international SPHERIC workshop*, June 2014. Paris, France.

[16] Goda, Y (1970). A synthesis of breaker indices. *Transactions of the Japan Society of Civil Engineers*, 2(2):227-230.

[17] Dean, R.G. and Dalrymple, R.A. (1991). Water wave mechanics for engineers and scientists. *Advanced series on ocean engineering*. World Scientific.

[18] Peregrine D.H (2003). Water-wave impact on walls. *Annu. Rev. Fluid Mech., 35*:23-43.

[19] Peregrine, D. H., and L. Thais. "The effect of entrained air in violent water wave impacts." Journal of Fluid Mechanics 325 (1996): 377-397.

[20] Bredmose H, Peregrine DH, Bullock GN. 2009 Violent breaking wave Impacts. II. Modelling the effect of air. J. Fluid Mech. 641, 389–430